E3S Web of Conferences **730**, 03015 (2026) https://doi.org/10.1051/e3sconf/202673003015
Soft Soils 2026

An updated explicit approach to account for undrained cyclic loading effects in offshore monopile foundations

Ilaria Del Brocco[1*], *Ronald B.J.* Brinkgreve[2], and *Tuan* Bui[1]

[1] Seequent – The Bentley Subsurface Company, Delft, The Netherlands
[2] Department of Geoscience and Engineering, Delft University of Technology, Delft, The Netherlands

Abstract. Cyclic loading, for example on offshore monopile foundations, affects the bearing capacity compared to static conditions. Rather than simulating the full loading history, the capacity under cyclic loading can be evaluated using an explicit approach, where loads and soil response are expressed as a function of the number of cycles. Along this line, the Norwegian Geotechnical Institute has developed a cyclic accumulation procedure to derive target stress-strain curves, which can be fitted with appropriate constitutive models for the modelling of offshore foundations in the finite element method. A simplified version of this procedure, known as UDCAM-S (which uses the NGI-ADP constitutive model in the background), has been implemented in the finite element code PLAXIS. This procedure has been recently updated to account for different levels of shear strength moblization along a monopile. It employs an iterative procedure where the seabed is divided into several sub-layers, each with its own load history and corresponding parameter set. The NGI-ADP model parameters are fitted to target curves for triaxial compression, extension, and direct simple shear, using a Particle Swarm Optimization algorithm. To speed up the optimization process, a fast surrogate model, pre-trained on tens of thousands of single stress-point laboratory test simulations, was developed. This results in an efficient procedure that provides a more realistic representation of the seabed response for the design of offshore monopile foundations under undrained cyclic loading conditions.

1 Introduction

Structures, and their foundations in/on the ground, are subject to natural loading conditions, which often have a cyclic character. Earthquakes are probably the first type of cyclic loading one would think of, but also wind and sea waves around offshore structures are a major source of natural cyclic loads that need to be considered in design calculations.

To incorporate cyclic loading effects in numerical analysis for the design of offshore foundations (apart from dynamic components such as inertia and damping), an *implicit* or *explicit* approach can be followed. The implicit approach would require numerically simulating every load cycle while using a soil constitutive model that accounts for the accumulation of plastic strains and pore pressures in every cycle (e.g. [1-3]). The implicit approach is computationally intensive when over 100 cycles need to be considered in 3D numerical analysis. Such an approach may not be practical in the daily design of offshore projects.

The explicit approach assumes a simplified description of the loads (usually non-symmetric and irregular) as an ordered set of constant amplitude cyclic loads ('load history'). Loads and soil response are expressed in terms of cyclic and average components as a function of the number of load cycles. In this way, the effects of cyclic loading and strain/pore pressure accumulation can be analysed in static monotonic analyses. Examples of explicit approaches are the constitutive models presented in, amongst others, [4, 5].

Based on earlier work by Anderson (e.g. [6, 7], the Norwegian Geotechnical Institute (NGI) has developed explicit methods for numerical analysis and design of offshore foundations ([8-11]). For clay-type soils exhibiting pure undrained behaviour, the UnDrained Cyclic Accumulation Model (UDCAM) has been developed ([12]). A simplified version of this model called UDCAM-S was implemented in the PLAXIS finite element code ([13, 14]) and is available for practical design of offshore foundations. However, the existing implementation of UDCAM-S is not very suitable for the design of offshore monopiles. This is because the underlying assumption that the shear stress in the entire soil domain is proportional to the loads ignores stress redistribution and differences in strength mobilization around the monopile in reality. Therefore, an updated procedure was developed, taking account of different load histories around the monopile, from mudline to pile tip. This paper describes various aspects of this updated procedure.

Section 2 of this paper focuses on undrained cyclic accumulation. It first describes the procedure incorporated in the existing UDCAM-S model, followed by the updated approach. Part of this new procedure involves the way how constitutive model parameters are

* Corresponding author: ilaria.delbrocco@bentley.com

optimized based on target stress-strain curves. To speed up the optimization process, a surrogate model was developed, which is also described in this section. Section 3 shows an example demonstrating the use of the updated UDCAM-S model in a practical application. The paper ends with a discussion and the main conclusions of the research related to the updated model.

2 Undrained Cyclic Accumulation

One key aspect of the explicit methods developed by NGI is the use of stress-controlled static and cyclic triaxial compression (TXC), extension (TXE), and direct simple shear (DSS) tests to investigate the soil behaviour under cyclic loads. The reader is referred to earlier publications by (amongst others) [9] for details and definitions of the various terms and quantities. These tests are performed with a constant average shear stress component τ_a (due to principal stress difference in the initial state and the increment $\Delta\tau_a$ applied in a static phase), while the cyclic shear stress component τ_{cy} is applied (Fig. 1). For clays, the results of each test are described in terms of average and cyclic strain components as a function of the number of cycles (N). The results (γ_{cy} and γ_a) are mapped in the form of contour diagrams (Fig. 2) whose axes represent the test conditions (τ_a, τ_{cy}, and N). Also, key in the NGI explicit method is that the nonlinear relationship between γ_{cy} and γ_a as a function of the combination of τ_a and τ_{cy} is directly extracted from the diagrams as a function of N. Given an ordered set of constant amplitude cyclic loads, the diagrams are used to identify an equivalent number of cycles (N_{eq}) of the highest amplitude, producing the same effect as the load history. By taking a cross section of the 3D strain contour diagrams at a certain N_{eq}, the resulting 2D contour diagram can be intersected by the 'path' (i.e. ratio of cyclic to increment of average shear stress, $\tau_{cy} / \Delta\tau_a$), to extract target stress-strain curves in TXC, TXE and DSS, representing the monotonic equivalent to the entire load history. The curves can be considered in terms of cyclic, average or total (average + cyclic) stress-strain curves.

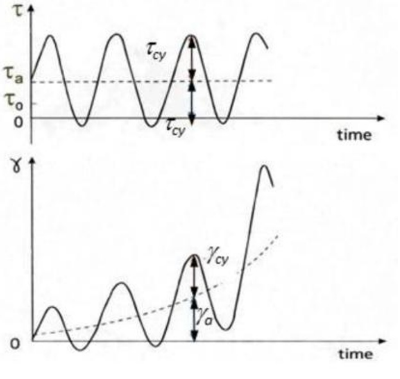

Fig. 1. Definition of average and cyclic shear stress, and corresponding strain diagram (after [12]).

The target curves are used to calibrate a constitutive model, optimizing its parameter values to achieve the best fit with simulated laboratory test results. In essence, this is the procedure followed by the UDCAM model ([12]), where the underlying soil constitutive model is similar to the NGI-ADP model ([15]). Note that for a given design storm, the load history (and consequently N_{eq}) and the 'path' are non-uniform, but vary by location in the soil domain, since soil closer to the foundation experiences greater disturbances than soil further away. Hence, in numerical analysis, the UDCAM procedure should be ideally applied separately at each stress point, but this is computationally intensive and impractical.

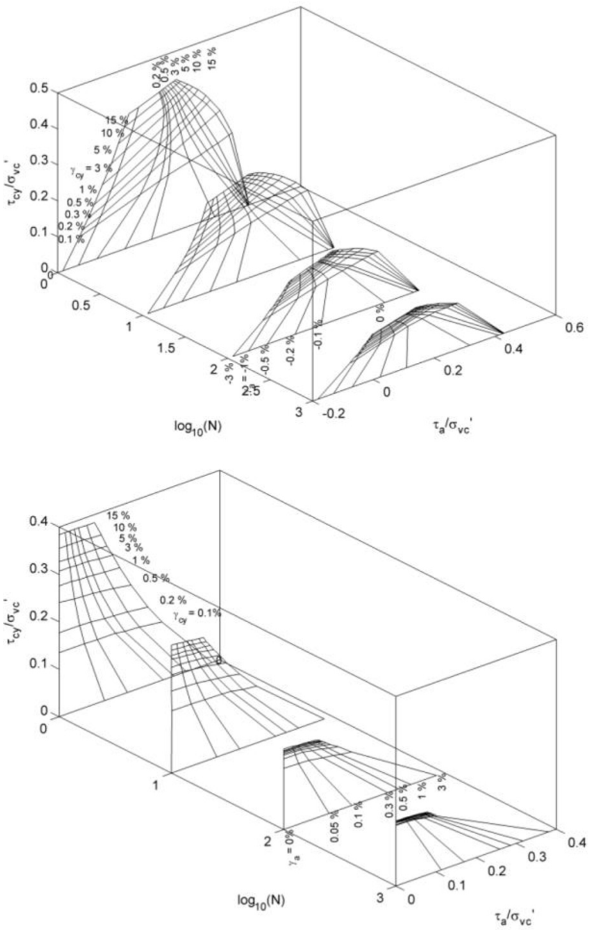

Fig. 2. Example of 3D strain contour diagrams (after [17]).

2.1 Existing simplified UDCAM procedure

In the existing UDCAM-S procedure, a single value of N_{eq} is determined for the entire soil around the foundation element, assuming the strength mobilization is uniform and proportional to the mobilization of the full foundation capacity. With this hypothesis, the calculation of N_{eq} is based on the ratio of global mobilization levels from the load parcels with respect to the maximum load. To calculate N_{eq}, the cyclic strain procedure ([9]) is performed in the cross section of the DSS contour diagram for $\tau_a = 0$, which results in an N_{eq}-value at failure (defined at γ_{cy} = 15%). The corresponding stress-strain target curves for a given loading path are extracted in cross sections taken at N_{eq} and the parameters of the UDCAM-S constitutive model are subsequently optimized using Particle Swarm Optimization (PSO) ([16]).

Since this procedure is carried out for the entire soil domain using global forces rather than local load histories, it can be performed as pre-processing. The resulting constitutive model parameters are assigned to the entire soil domain. A static numerical analysis with monotonic loading is then performed to simulate the equivalent results of the full cyclic load history.

Although this procedure has been widely adopted by the offshore industry due to its simplicity, the consideration of only one set of parameters for the entire soil domain makes it less suitable for monopile foundations. In this scenario, pile deflection and rotation due to lateral loads and bending moments coming from super-structure involves different mobilization levels along the monopile, mostly below the soil's local capacity. This requires a modification of the original N_{eq} calculation procedure to account for the more realistic varying mobilization levels.

2.2 Updated UDCAM-S

To compromise between the expensive original UDCAM and the more simplistic UDCAM-S procedures, an intermediate solution has been explored by applying the entire procedure on a limited number of soil (sub-)layers (e.g. every few meters depth; [17]), optionally within a certain radius around the monopile (e.g. one time the monopile diameter, *D*).

It is assumed that a first static analysis is performed with an initial set of static parameters in each layer. The initial shear strength profile will be used in every iteration to de-normalize the target curves.

Since the load history in each layer is not known a priori, the application of the cyclic accumulation procedure with local load histories requires the results of a finite element (FE) analysis, namely the soil reactions in each layer, to identify the local mobilization levels and N_{eq}. Constitutive model parameters to be used in the FE analyses should be derived from N_{eq}, while the change of parameters may lead to a redistribution of stresses, local mobilization levels and N_{eq}. Hence, the updated UDCAM-S approach introduces an iterative procedure in which FE analyses and cyclic accumulation are performed in conjunction with each other. The first iteration could either start from an initial guess of N_{eq}, or from N_{eq} calculated from the load ratios of the static analysis. When updating the parameters after each iteration, the solution tends to converge within a small number of iterations (3-10).

Additionally, the updated UDCAM-S procedure as described herein includes a modified N_{eq} calculation, the enhancement of the calculation of the updated parameters, and further automations. While the existing UDCAM-S procedure requires the user to provide valid ranges of parameter values as search space for the optimization, the current model does this automatically.

The complete set of UDCAM-S model parameters in relation to the NGI-ADP parameters is listed in Table 1. While NGI-ADP considers the static undrained shear strengths, s_u, UDCAM-S involves the undrained shear strengths, τ, corrected for cyclic accumulation effects.

Table 1. Set of NGI-ADP and UDCAM-S model parameters.

NGI-ADP	UDCAM-S	Description
ν_u	ν_u	Undrained Poisson's ratio
s_u^A	τ^C	Undrained shear strength in TXC
G_{ur} / s_u^A	G_{ur} / τ^C	Unload/reload shear modulus ratio
s_u^E / s_u^A	τ^E / τ^C	Undr. shear strength ratio in TXE/TXC
s_u^{DSS} / s_u^A	τ^{DSS} / τ^C	Undr. shear strength ratio in DSS/TXC
γ_f^C	γ_f^C	Equivalent failure shear strain in TXC
γ_f^E	γ_f^E	Equivalent failure shear strain in TXE
γ_f^{DSS}	γ_f^{DSS}	Failure shear strain in DSS
τ_0 / s_u^A	τ_0 / τ^C	Initial strength mobilization ratio

Note: In NGI-ADP, active undrained strength, s_u^A, is used, where s_u^A is assumed 0.99 s_u^C

Some parameters are directly derived from the target stress-strain curves and the contour diagrams:

τ^C, τ^E/τ^C, τ^{DSS}/τ^C: extracted from target curves.

$\tau_0 / \tau^C = \tau_0 / s_u^A$: read from the contour diagram.

The remaining parameters are optimized considering the following ranges:

G_{ur} / τ^C : [50, 500]

γ_f^C : $[\tau^C (\tau^C - \tau_0)/ 50, max]$

γ_f^E : $[\tau^E (\tau^E + \tau_0)/ 50, max]$

γ_f^{DSS} : $[\tau^{DSS} (\tau^{DSS})/ 50, max]$

The maximum failure strain in the search range (*max*) is taken as the strain where a plateau in the respective target stress-strain curve is reached, or simply the maximum strain if a plateau cannot be identified. The latter may be the case for highly over-consolidated clays where large (cyclic and/or average) strains (>15%) would be required to mobilize the cyclic shear strength.

Using these ranges, model parameters are optimized by comparing the results of lab test simulations to the target curves for each 'particle' in PSO. The lab tests involve anisotropic initial stress conditions in TXC, TXE and DSS where the vertical effective stress σ'_v = 50 kN/m², the horizontal effective stress $\sigma'_h = K_0 \sigma'_v$ and

$$K_0 = 1 - 2\ (\tau_0 / s_u^c)\ (s_{u,d}^c / \sigma'_v) \tag{1}$$

where τ_0 / s_u^c is obtained from the contour diagram and $s_{u,d}^c / \sigma'_v$ is the static *S*-ratio, given as an input parameter.

If the behaviour is assumed isotropic, only γ_f^{DSS} and G_{ur} / τ^C are optimised, while $\tau^C = \tau^E = \tau^{DSS}$ and $\gamma_f^C = \gamma_f^E = \gamma_f^{DSS}$.

The whole process includes the following tasks / components:

1. Cyclic strain accumulation procedure to find the equivalent number of cycles (N_{eq}) for a given load history based on strain contour diagrams for the relevant type of clay.
2. Determination of target stress-strain curves for the calculated N_{eq} based on a provided 'path' in the stress-strain contour diagrams.
3. Particle swarm optimization to best fit the UDCAM-S model parameters to the target curves.
4. Calculating local load ratios using the soil reactions and the capacity of the layers.
5. User-interface dealing with the required input/output data and interactive tasks.

Ad 1. N_{eq} corresponding to the actual strength mobilization in each layer is calculated by entering Anderson's accumulation procedure with the load ratio defined by the maximum soil reaction in that layer and the layer capacity, p_f, approximated as:

$$p_f = 9\, s_u^C\, D \qquad (2)$$

Although this updated procedure is less computationally demanding than the full UDCAM procedure, the required number of lab test simulations are still significant. Note that each step of a ‘particle’ in PSO requires three stepwise iterative lab test simulations on a single stress point and the subsequent comparison with the respective target curve. A ‘particle’ in this context is a set of parameter values. Typically, 25-100 particles and 25-100 steps per particle are used to find an optimized set of parameter values for a single layer, while the updated UDCAM-S procedure considers typically up to 10 layers and 3 to 10 global iterations (i.e. complete 3D finite element calculations) to find an overall converged solution. Hence, in the order of 10^6 lab test simulations may be required in addition to the 3D FE calculations.

2.3 Surrogate model

To accelerate the updated UDCAM-S procedure, a surrogate model was created to produce stress-strain curves for all three test types for a given set of model parameters. The surrogate model considered here is an artificial neural network with intermediate hidden layers (Multi-Layer Perceptron, MLP). Input features of the MLP are the UDCAM-S model parameters and output features are the corresponding scaled stress-strain curves represented by 3 x 101 pairs of values, i.e. 606 output features in total. Further optimization of the number of output features to reduce the training time was not the objective of this work and will be studied in future research. Scaling of stress-strain curves is done by dividing any stress value by the cyclic undrained shear strength in triaxial compression, τ^C, to condition the output features and to obtain a more accurate surrogate model. The input and output data are further scaled using the StandardScaler function in the Python module Scikit Learn. Between the 10 input features and the 606 output features, the MLP involves three hidden layers of 64, 256 and 512 neurons, respectively. The model and its data structure are designed to deal with multiple samples at once, and to make use of the GPU (via the CUDA library) to gain optimum performance when used in the context of parameter optimization.

The surrogate model was trained on a dataset of 47500 parameter sets and corresponding results obtained from single stress point lab test simulations (3x101 stress-strain pairs from TXC, TXE and DSS). 80% of the data was used for training; 20% for testing. A (visual) check on random samples of unseen parameter sets shows that the surrogate curves almost perfectly match the curves obtained from lab test simulations.

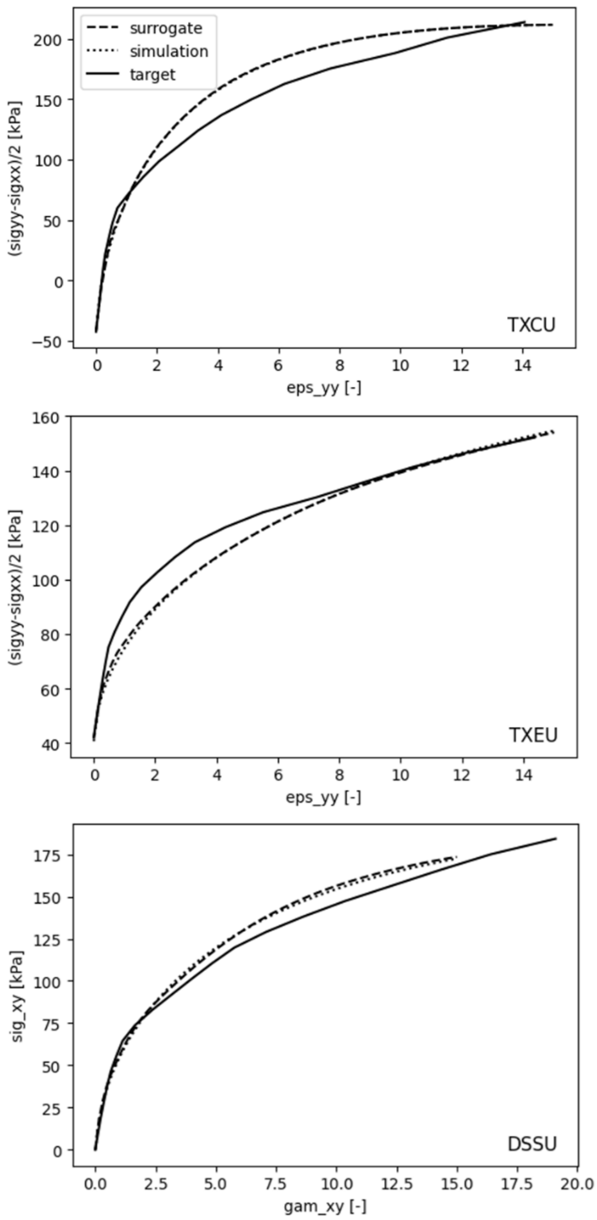

Fig. 3. Comparison between target curve, model simulation.

Instead of directly using the UDCAM-S model parameters in the optimization, seven independent parameters $\{\xi_1, ..., \xi_7\}$ with values in the range [0,1] were used, relating to the model parameter ranges as considered in the PSO algorithm:

ν = 0.495 (undrained behaviour)
τ^C = *select* (ξ_1, 5, 100)
G_{ur} / τ^C = *select* (ξ_2, 50, 1000)
τ^P / τ^C = *select* (ξ_3, 0.03, 2.3)
τ^{DSS} / τ^C = *select* (ξ_4, 0.3, 2.3)
γ_f^C = *select* (ξ_5, 400, 2000) / (G_{ur} / τ^C)
γ_f^E = *select* (ξ_6, 0.95, 5.0) • γ_f^C
γ_f^{DSS} = *select* (ξ_7, 0.95, 5.0) • γ_f^C
τ_0 / τ^C = 0.5 (1 - K_0) σ'_v / τ^C
(K_0 as obtained from the contour diagram)

The *select* function returns an interpolated value between the second and third parameter in the list based on the independent parameter ξ_i.

In this way, correlations between model parameters can be accounted for and the model is well conditioned.

The PSO algorithm was adapted to benefit from the specific surrogate model design in which all curves from all samples ('particles') are produced at once rather than treating each 'particle' or each curve individually. A total of 100 'particles' and 30 steps were found to give fast and accurate results when using PSO with the trained surrogate model to optimize the model parameters against the target curves. Fig. 3 shows an example of a surrogate model fit (dashed line) on three target curves (solid line), together with the numerical lab test simulation of the optimized parameter set (dotted line). The latter almost fully coincides with the surrogate. It demonstrates the quality of both the fitting algorithm and the surrogate model.

3 Example

In this section an example, based on [17], is elaborated with the updated UDCAM-S procedure.

3.1 Model setup

A steel tubular monopile is installed in a homogeneous clay-type soil with embedded length $L = 45$ m, diameter $D = 5.2$ m and wall thickness $t = 54$ mm. Due to symmetry, only half of the problem is modelled, with lateral dimensions 12 D (62.4 m) from the monopile centre line and a depth extending to 3 D (15.6 m) below the pile tip. Shell elements with steel properties were used to model the monopile rather than using solid elements as in the earlier publication [17]. Elastic interface elements with normal and shear stiffness $k_n = k_s = 10^6$ kN/m^3 are used around the pile; these are not intended to realistically model the pile-soil interaction, but rather to extract the contact stresses to determine the strength mobilization ratio per layer.

The soil, as reported in [12] for the same case, has a total unit weight $\gamma = 18$ kN/m^3 ($\gamma' = 8$ kN/m^3 in the seabed), while the undrained shear strength profile is defined by $s_u^{DSS} / \sigma'_{v0} = 0.35$, where σ'_{v0} is the initial vertical effective stress, with strength anisotropy ratios $s_u^{DSS} / s_u^C = 0.9$ and $s_u^E / s_u^C = 0.45$. Considering ULS conditions, a partial material factor of 1.25 is applied to the shear strength values. Isotropic properties are used, considering an average shear strength $s_u^{ISO} = (s_u^C + s_u^E + s_u^{DSS}) / 3$, giving an undrained shear strength increment $s_u^{ISO}{}_{inc} = 1.95$ kN/m^2 per meter depth in ULS conditions. The initial shear strength mobilization, $\tau_0 / s_u^A = 0.7689$, is based on the triaxial strain contours.

The initial failure strain $\gamma_f = 3\%$ and soil stiffness ratio $G_{ur} / s_u^{AV} = 1000$ were determined based on the pure average (i.e. 'horizontal' path) stress-strain curve extracted from the DSS contour diagram for $N_{eq} = 1$, which is assumed as an approximation of the monotonic response.

Assuming that the soil is normally consolidated, a K_0 of 0.625 is used, following Eq. (1).

The contour diagrams, in the original paper, normalized by the vertical effective stress σ'_{v0}, were converted here to diagrams that are normalized by the static undrained shear strength in triaxial compression, s_u^C, using the aforementioned ratios.

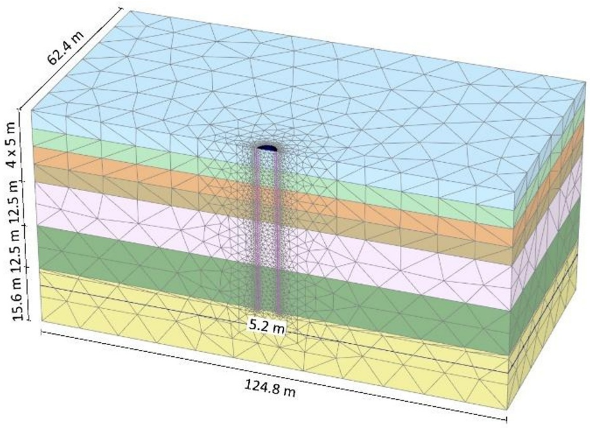

Fig. 4. 3D finite element mesh of the problem.

Around the monopile, six sub-layers were defined, as in [17]: the upper four layers having a thickness of 5 m each, and the lower two layers a thickness of 12.5 m.

The 3D FE mesh of medium global density was refined by a factor 0.25 in a zone 1 times the diameter (1 D) around the monopile, and further refined by a factor 0.05 within 0.1 D. The mesh consists of a total of 39510 10-node tetrahedron elements, 2771 6-node shell elements and 2780 12-node interface elements. To better visualize the displacements and check the monopile structural forces, 'soft beams' were placed vertically at the front and rear of the monopile. Fig. 4 shows the 3D FE mesh.

To apply the load properly, a rigid body element was applied over a slightly elevated top ring of the monopile (leaving a small gap between the rigid body and the top of the seabed). The maximum load, representative of a relevant storm, multiplied by a ULS partial factor of 1.35, and divided by 2 accounting for simulating half the problem, gives a maximum vertical force $F_{v,max} = 6145$ kN, a horizontal force $F_{h,max} = 2856$ kN, and a bending moment $M_{max} = 107443$ kNm. Following the description [17], all force components were applied at the rigid body reference point at the top of the monopile, considering their respective proportions as listed in Table 2. Standard fixities are applied at the model boundaries (rollers at the vertical sides and a fully fixed bottom).

Besides the initial phases, including the initial static stress generation and the monopile installation as 'wished-in-place', eleven subsequent phases are defined, reflecting the loads in the various load parcels. Table 2 shows the load parcels in terms of load fractions and corresponding number of cycles.

An initial value for N_{eq} was calculated using the first part of the existing UDCAM-S procedure with the global load history from Table 2. This value ($N_{eq} = 18$) was used as an initial guess for all six layers to obtain the corresponding parameter sets (Table 3, Degraded) in 'iteration 0' of the analysis. The layer below the monopile retains its original static properties (Table 3, Static), assuming that the contribution of the pile base to the overall capacity is limited in this case of a relatively slender pile.

Table 2. Load parcels.

Parcel	F/F_{max}	N
1	0.2	900
2	0.37	500
3	0.49	200
4	0.58	90
5	0.64	50
6	0.7	30
7	0.77	15
8	0.83	8
9	0.89	4
10	0.96	2
11	1.00	1

Table 3. Initial set of degraded and static model parameters.

Symbol	Degraded	Static	Unit
ν_u	0.495	0.495	-
τ^C_{ref}	0.07671	0.1	kN/m^2
τ^C_{inc}	1.496	1.95	kN/m^2/m
G_{ur} / τ^C	451.2	1000	-
τ^E / τ^C	1	1	-
τ^{DSS} / τ^C	1	1	-
γ_f^C	11.68	3	%
γ_f^E	11.68	3	%
γ_f^{DSS}	11.68	3	%
τ_0 / τ^C	0.7689	0.7689	-

The new UDCAM-S user interface detects all cyclic phases representing the individual load parcels and allows the number of load cycles to be specified. It further allows specifying all necessary input data and runs the calculations automatically.

After the complete 3D FE analysis with the initial degraded parameter set ('iteration 0'), all calculation phases are repeated with updated parameter sets for all layers from the updated UDCAM-S procedure in subsequent iterations, while intermediate results are stored. The iteration process is completed if converged values of N_{eq} in all layers have been obtained.

3.2 Results

The results of the last (7th) iteration from the complete analysis in terms of monopile lateral displacement, bending moment and shear force, are plotted over the results from [17] and the original UDCAM results from [12] (Fig. 5). The automatically extracted bending moments at the top of each (sub-) layer are indicated by the small 'o'-symbols in the diagram ('shell' in the legend). As an alternative, bending moments were calculated back from the axial deformations in the 'soft beams' ('beams' in the legend). The shear forces were calculated as derivatives from the bending moments. The results show overall good agreement.

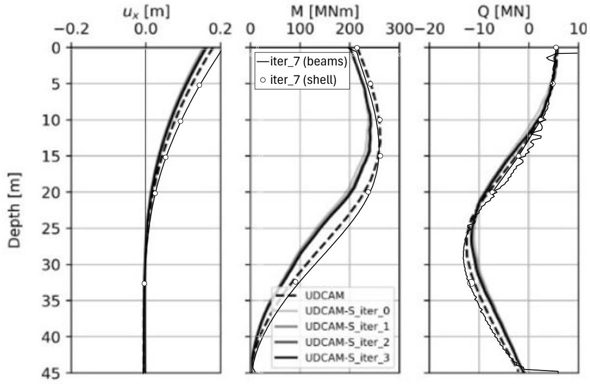

Fig. 5. Comparison of results with [17] and [12].

Fig. 6a shows the evolution of N_{eq} per layer. Starting from a uniform value of N_{eq} = 18 in iteration 0, some layer values increase and some decrease, but they stabilize after seven iterations. The value for L1 increases to a maximum of 712, while the layers below arrive at lower values of N_{eq} (L2: 167; L3: 75; L4: 9.8; L5: 1; L6: 1). This suggests that the top layer suffers most from cyclic strength degradation, which seems plausible.

Fig. 6b shows the evolution of the cyclic component of the maximum soil reaction force in each layer, $p_{cy,max}$, over the static layer capacity, p_f, as defined in Eq. (2). This ratio indicates how much of the static soil strength is mobilized in each layer. The mobilization ratios gradually change during the iteration process as a consequence of shear strength degradation (which differs per layer) and redistribution of the load. Also, this stabilizes after some iterations. Although it is tempting to assume that the top layer (L1) always has the highest mobilization ratio, this layer suffers most from the strength reduction. The final mobilization cannot exceed the reduced strength. This explains why the mobilization in L1 can be less than in L2, etc. The lowest mobilization is in the layer around the monopile rotation point (L5), while the bottom layer (L6) has a slightly higher mobilization due to movement in the 'passive' direction.

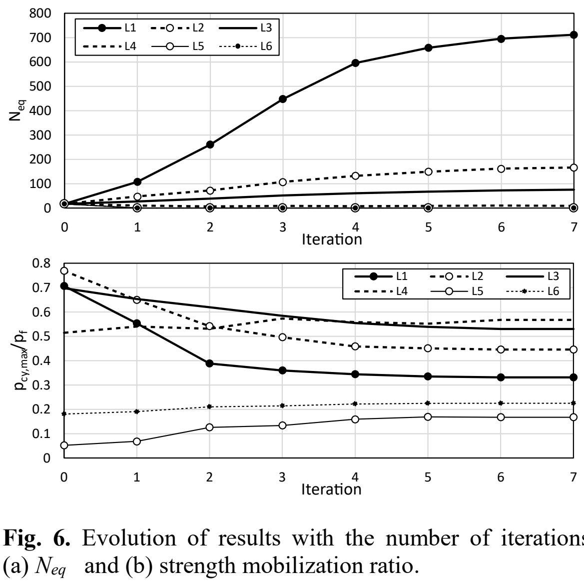

Fig. 6. Evolution of results with the number of iterations: (a) N_{eq} and (b) strength mobilization ratio.

4 Discussion

Based on the results presented in Section 3, there are a few discussion points that need further attention.

The first point relates to the use of interface elements around the monopile. This helps to obtain more accurate contact stresses to derive the mobilization ratios in the various (sub-)layers, provided the finite element mesh is sufficiently fine. However, it is important to prevent the variation of interface element properties between iterations. Therefore, it is important to ensure that the interface properties are independent of the (changing) parameter sets in the surrounding soil to avoid risks of oscillation and non-convergence in the iterative process.

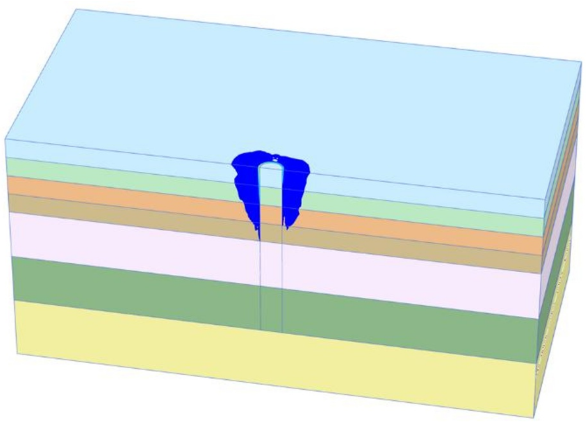

Fig. 6. Deviatoric strain contours (γ_s) around the monopile for γ_s > 1%, with a maximum $\gamma_{s,max}$ = 41.24%.

The second point concerns the size of the zone around the monopile in which parameters are updated. By looking at the contour plot of shear strains from the model (Fig. 6) it can be seen that significant shear strains (γ_s > 1%,) occur within the blue zone, whose size is approximately one diameter around the monopile. It might be more logical to update properties only within this high-shear zone rather than in the entire layer, which is also more consistent with the full UDCAM procedure. How much strain is considered 'significant' in this context, is subject to further discussion.

The last point is on the use of the surrogate model in conjunction with the PSO optimization process. The surrogate helps improving the performance of the optimization and thereby reduces the calculation time of the whole UDCAM-S procedure, provided the surrogate model is well trained and accurately represents the underlying stress-strain response obtained from lab test simulations. Some attention points:

- Using independent parameters allows for incorporating correlations between the actual model parameters.
- It helps to integrate the surrogate model within the PSO algorithm to deal with multiple 'particles' (parameter sets) at once, to gain optimum performance.
- Further optimization of the surrogate can be achieved by replacing the discretized stress-strain curves as output features by fitting parameters of functions representing those curves.

Despite the performance improvement when using the surrogate model, the overall calculation time of the UDCAM-S procedure is dominated by the 3D finite element calculations.

5 Conclusions

Following a recent publication on explicit modelling of cyclic loading of offshore monopile foundations, an improved automated procedure was developed. This procedure can be regarded as an update of the simplified UDCAM-S concept with the following improvements:

- Use of different (sub-)layers to differentiate in load histories, soil strength mobilization levels, and, consequently, different degradation levels of soil strength along the monopile.
- Allowing for load redistribution and convergence of degradation levels by introducing a stepwise (iterative) calculation process.
- Optional use of a fast surrogate model integrated in a particle swarm optimization algorithm, reproducing stress-strain diagrams that would otherwise be obtained from lab test simulations.

The updated UDCAM-S procedure was successfully applied in an example of a monopile subjected to a design storm. The results demonstrate the convergence of the calculation process. Results were found to be similar as reported in earlier publications. Based on the experiences acquired in this research some discussion points were raised.

References

1. H. Liu, J. A. Abell, A. Diambra, F. Pisanò, Modelling the cyclic ratcheting of sands through memory-enhanced bounding surface plasticity. Géotechnique, **69**, 783–800 (2019). https://doi.org/10.1680/jgeot.17.P.307.
2. H. Liu, J. A. Abell, F. Pisanò, Memory-enhanced plasticity modeling of sand behavior under undrained cyclic loading. J. of Geotech. Geoenviron. Eng., **146**, No. 11 (2020). https://doi.org/10.1061/(ASCE)GT.1943-5606.0002362
3. M. Yang, M. Taiebat, Y.F. Dafalias, SANISAND-MSf: a sand plasticity model with memory surface and semifluidised state.. Géotechnique, **72**, 227–246. (2022) doi: https://doi.org/10.1680/jgeot.19.P.363
4. A. Niemunis, T. Wichtmann, & T. Triantafyllidis, A high-cycle accumulation model for sand. Comput. Geotech. **32**, 245–263 (2005) https://doi.org/10.1016/j.compgeo.2005.03.002.
5. M. Achmus, M., Y-S. Kuo, K. Abdel-Rahman Behaviour of monopole foundations under cyclic lateral load. Comput. Geotech. **36**, 725-735. (2009). https://doi.org/10.1016/j.compgeo.2008.12.003
6. K.H. Andersen Behaviour of clay subjected to undrained cyclic loading. Proc. 1st Int. Conf. on the Behaviour of Offshore Structures, BOSS'76, Trondheim 1, 392-403. (1976).
7. K.H. Andersen, A. Kleven, and D. Heien. Cyclic soil data for design of gravity structures. J. Geotech. Eng. **114**: 517–539. (1988).

https://doi.org/10.1061/(ASCE)0733-9410(1988)114:5(517).

8. H.P Jostad and L. Andresen A FE procedure for calculation of displacements and Capacity of foundations subjected to cyclic loading. Proceedings for COMGEO I, Juan-les-Pins, Cote d'Azur, France. (2009).
9. K.H. Andersen. Cyclic soil parameters for offshore foundation design. Frontiers in Offshore Geotechnics III, 5–82. Editor. Vaughan Meyer. (2015).
10. H.P., Jostad, G. Grimstad, K.H. Andersen, and N. Sivasithamparam. A FE procedure for calculation of cyclic behaviour of offshore foundations under partly drained conditions. Front. Offshore Geotech. III 1 (May): 153–172. (2015).
11. H.P. Jostad, H. Liu, N. Sivasithamparam, R. Ragni, Cyclic capacity of monopiles in sand under partially drained conditions: a numerical approach. J. Geotech. Geoenviron. Eng., **149**, 1-12 (2022) DOI: 10.1061/JGGEFK.GTENG-10435.
12. H.P. Jostad, G. Grimstad, K.H. Andersen, M. Saue, Y. Shin, D. You. A FE procedure for foundation design of offshore structures–applied to study a potential OWT monopile foundation in the Korean Western Sea. Geotech. Eng. J. of the SEAGS & AGSSEA, **45**, 63-72 (2014). https://doi.org/10.14456/seagj.2014.7
13. Plaxis, 2018. PLAXIS reference manual
14. Seequent, 2025. PLAXIS reference manual
15. G. Grimstad, L. Andresen, H.P. Jostad. NGI-ADP: Anisotropic shear strength model for clay. Int. J. Num. Anal. Meth. Geomech., **36**: 483-497 (2012). https://doi.org/10.1002/nag.1016
16. J. Kennedy, R. Eberhart. Particle Swarm Optimization. Proceedings of IEEE International Conference on Neural Networks. Vol. IV. 1942–1948 (1995). doi:10.1109/ICNN.1995.488968
17. R. Ragni, N. Sivasithamparam, H.P. Jostad, Y. Zhang, T. Okuno, H. Sugiyama, K. Fukutake. Efficient modelling of cyclic degradation in monopile design. 9th Int. Conf. on Offshore Site Investigation Geotechnics, London, 1050-1056 (2023). doi:10.3723/NYJT4115.